Dynamic Frequency-Constrained Adaptive Coordinated Expansion Planning (DFC-ACEP)

Mohamed Elnasry, Colin Christy, James D. McCalley, Venkataramana Ajjarapu
Department of Electrical and Computer Engineering
Iowa State University, Ames, IA, USA
Email: mayman@iastate.edu

***Abstract*—The increasing penetration of inverter-based resources (IBRs) and the gradual displacement of synchronous generators (SGs) are leading to reduced system inertia, posing significant challenges for frequency stability. This paper explores the impact of reduced inertia on power system frequency dynamics and formulates a minimum inertia constraint within an Adaptive Coordinated Expansion Planning (ACEP) framework. The proposed dynamic frequency constraints (DFCs) ensure sufficient inertial and primary frequency response to mitigate large frequency deviations following disturbances. Case studies illustrate the necessity of integrating inertia constraints into long-term transmission and generation expansion planning.**

I. Introduction

Traditional expansion planning methodologies primarily focus on optimizing generation capacity without incorporating constraints that assess system dynamics. This approach assumes that generation adequacy alone guarantees system reliability, overlooking the crucial role of frequency stability assuming pre-configured dynamic characteristics of system devices [1]. As the generation mix shifts toward a greater share of low-cost, zero-carbon renewable energy sources with inherently low or zero inertia, the power system's ability to effectively respond to disturbances is significantly deteriorated. This shift necessitates a paradigm change in expansion planning, where frequency security constraints must be embedded to ensure the system remains resilient under future operating conditions.

Convenient synchronous generators have provided short-term frequency stability by supplying inertia and primary frequency control (PFR), slowing frequency deviations following disturbances. As IBRs increasingly displace synchronous machines, system inertia declines, resulting in higher rates of change of frequency (RoCoF), lower frequency nadirs, and secondary frequency nadirs, increasing the risk of instability. To maintain frequency stability, power system planning must ensure adequate levels of inertia and PFR. While IBRs can provide inertia-like and PFR-like capabilities, their response mechanisms differ from synchronous machines. Most IBRs lack rotational inertia but leverage fast frequency response (FFR) to inject power during frequency deviations. Depending on the technology, FFR can either mimic the instantaneous effect of inertia or provide sustained PFR. Wind turbines can temporarily increase output by extracting excessive kinetic energy from using their rotating blades, whereas battery energy storage systems (BESS) offer both rapid injection and sustained support. Table I summarizes the frequency response capabilities of different generation technologies.

The effectiveness of inverter-based resources (IBRs) is highly dependent on their control strategy, with grid-forming (GFM) inverters providing rapid stabilization, while grid-following (GFL) inverters exhibit inherent delays due to their reliance on real-time system measurements. A major challenge lies in accurately quantifying the equivalent inertia and ramping capabilities of IBRs across various control schemes. However, such characterization is not feasible during the planning stage and, if attempted, would lead to highly nonlinear dynamic programming formulations, significantly increasing computational complexity. Notably, the fast response of GFL-IBRs—the most widely deployed control type—occurs typically two to three times faster than that of synchronous generators. While this rapid response can enhance frequency containment, improper coordination of frequency support services may lead to unintended consequences, such as exacerbated system oscillations and secondary frequency dips even more severe than the initial nadir. Addressing this issue requires early-stage integration of stability-driven constraints into expansion planning to ensure a well-coordinated mix of generation technologies, thereby mitigating frequency-related risks.

The ACEP framework provides a structured approach for integrating DFCs into long-term power system planning. By incorporating these constraints, predefined frequency stability metrics can be systematically enforced through future generation investment decisions. The proposed DFC-ACEP framework enables investment strategies that enhance frequency resilience in evolving power grids. This is achieved through the precise characterization of frequency support services provided by various generation technologies and the explicit incorporation of these capabilities within the cost-optimization formulation, ensuring a balance between economic efficiency and system reliability.

II. Modeling of Frequency Security Constraints From Diverse generation Technologies

As fossil fuel-based generation retires but remains part of the system, it is essential to emphasize the need for frequency support from both conventional and renewable generation resources. This section first examines the various forms of frequency services provided by different technologies and control

TABLE I: Summary of Frequency Response Capabilities of Various Technologies

Resource	Inertia	PFR
Synchronous Generator	Yes	Yes
Synchronous Condenser	Yes	No
BESS	Yes	Yes
Wind (MPPT)	No	No
Wind + Inertia Emulation	Yes	No
Wind + BESS	Yes	Yes
Derated Wind	Limited	Limited
Solar PV (MPPT)	No	No
Solar + BESS	Yes	Yes
Derated Solar	Limited	Limited
Load Resources (LR)	No	Yes

schemes. Subsequently, we derive the necessary constraints to ensure the secure dynamic operation of the system under the largest contingency.

A. General Overview of Inertial and Primary Frequency Services

Following a disturbance, the system experiences a maximum RoCoF at the onset, dictated by the initial power imbalance. The inertial response of synchronous machines immediately limits RoCoF, slowing the frequency decline and arresting the nadir. As the system reacts, the PFR from synchronous and converter-based resources, along with the LDR, is activated. Given its rapid adjustability, converter-based PFR typically responds faster, while LDR can dynamically reduce demand, further mitigating frequency deviations.

Once the combined PFR and LDR compensate for the power imbalance, the inertial contribution diminishes, marking the nadir. To ensure that the frequency nadir remains within acceptable limits, the duration and magnitude of inertial response must be optimized to regulate kinetic energy release while rapidly engaging PFR and LDR. Thus, a coordination must be established between the target nadir, available inertia, PFR capacity, LDR flexibility, and ramping capability to ensure secure dynamic operation.

B. Primary Frequency Response From Governors

In order to meet the PFR requirement [2], each interconnection has a frequency response obligation, which is defined as the amount of increase in generation that must occur per unit of frequency decline (megawatts [MW]/hertz [Hz]). Also established is the maximum delta frequency (MDF) or the decline in frequency that results in full frequency response. The product of these two factors is the PFR obligation by interconnection. This interconnection frequency response obligation (IFRO) is further divided by BA in proportion to demand so that each region "shares" its obligation to the entire interconnection. Hence for individual generation resource we have:

$$\Delta P_i^{SG}(MW) = \frac{1}{D_i^{SG}} \frac{\Delta f(Hz)}{f_0} \times S_i^b \tag{1}$$

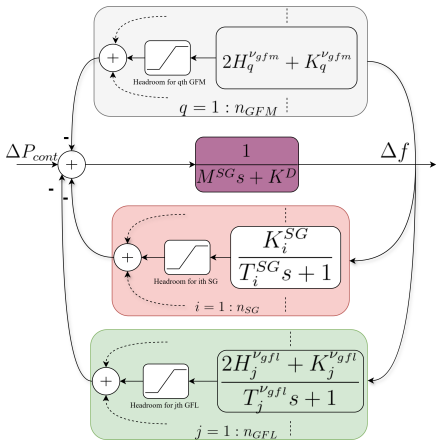

Fig. 1: Frequency Dynamics of the generation mix

S_i^b is the base MVA of the i^{th} synchronous machine, and $\Delta f(Hz)$ is the frequency deviation in Hz. Hence we have for all SGs,

$$\sum_i \Delta P_i^{SG} S_i^{b,SG} = \sum_i K_i^{SG} \Delta f \tag{2}$$

ΔP_i^{SG} is the synchronous machine output power change in pu.

We consider a generation fleet capable of providing Primary Frequency Response (PFR), emphasizing three distinct control strategies: synchronous generators, Grid-Following (GFL) inverter-based resources (IBRs), and Grid-Forming (GFM) inverter-based resources (IBRs) as shown in Fig.1. We assume each variable renewable energy (VRE) resource can operate under either GFL or GFM control strategies, with the flexibility to activate one or both of the power-frequency control loops—namely droop and inertia controls—if configured to support PFR. This is feasible by partially loading the VRE or with energy storage systems. Conversely, if an IBR operates at a constant energy output without active frequency-responsive controls, it cannot provide PFR, including inertial support, in response to grid disturbances. Now, denote the IFRO is the interconnection PFR obligation in MW/Hz and the corresponding obligation of a region (r) is denoted by $IFRO_r$ such that:

$$IFRO = \sum_r IFRO_r \tag{3}$$

Referring to (2), the PFR constraint considering the generation mix is re-formulated as (**PFR-Headroom constraint, i.e., different from the nadir constraint**):

$$\sum_{i \in r}^{n_{sg}} K_i^{SG} S_i^{b,SG} + \sum_{j \in r}^{n_{gfl}} K_j^{\nu_{gfl}} S_j^{b,\nu_{gfl}} + \sum_{q \in r}^{n_{gfm}} K_q^{\nu_{gfm}} S_q^{b,\nu_{gfm}} \geq IFRO_r \cdot f_0 \cdot \overline{\Delta f} \tag{4}$$

This obligatory PFR must be released when the frequency reaches its maximum allowable deviation $\overline{\Delta f}$. For instance $f_0 \times \overline{\Delta f} = 0.28Hz$ for the western interconnection.

Operating at a partially loaded level (or alternatively, curtailing energy) incurs a cost, as curtailed energy cannot be sold into the market. Thus, proper incentives must exist for variable generation to provide frequency response [3]. Given that said, this implies that maintaining PFR reserve imposes a cost that covers the need to keep the some units partially loaded to respond to frequency deviations and additional cost that cover the wear and tear that result due to the continuous active response of the generation unit to the grid conditions.

Moreover, the above mentioned IFRO requirement only accounts for the frequency deviation by implementing the droop control of the units, but do not account for the necessity of inertia energy support, i.e., the inertia loop that each IBR technology can utilize to mimic the synchronous behavior and arrest the frequency decay speed, i.e, limiting the RoCoF.

While synchronous inertia represents a physical property inherently available through the immediate release of kinetic energy stored in rotating masses, thereby mitigating the RoCoF, the scenario differs significantly for VREs interfaced via IBRs. For IBRs, both inertia-like response and PFR depend explicitly on reserved headroom capacity. Therefore, proper allocation of headroom in IBRs is essential, not only for delivering effective PFR but also for enabling a rapid yet non-instantaneous inertial-type response. This necessitates introducing an additional operational constraint specifically dedicated to ensuring sufficient IBR headroom to fulfill the inertia and frequency stability requirements. The constraint is mathematically expressed as in (5), and (6) explicitly accounting for its temporal dependency. A comprehensive derivation of this inertia-headroom constraint is provided in Appendix A. (**Inertia-Headroom constraint**) :

$$\sum_{j\in r}^{n_{gfl}} \Delta P_j^{\nu_{gfl}}(t) = \frac{\Delta P_{cont}}{MT}\mathcal{L}^{-1}\left\{\frac{(Ts+1)\left\{2\sum_{j\in r}^{n_{gfl}} H^{\nu_{gfl}} s\right\}}{s(s^2+2\zeta\omega_n s+\omega_n^2)}\right\} \tag{5}$$

$$\sum_{q\in r}^{n_{gfm}} \Delta P_j^{\nu_{gfl}}(t) = \frac{\Delta P_{cont}}{MT}\mathcal{L}^{-1}\left\{\frac{(Ts+1)\left\{2\sum_{q}^{n_{gfm}} H_q^{\nu_{gfm}} s\right\}}{s(s^2+2\zeta\omega_n s+\omega_n^2)}\right\} \tag{6}$$

C. FFR From IBRs

IBRs can be classified based on their capability to provide frequency support, particularly in terms of PFR and inertial response. Grid-forming inverters, developed through research led by PNNL and approved by WECC [4], regulate frequency deviations through a droop-based control strategy. Under a single-loop droop control scheme, these inverters modulate real power output in response to frequency deviations, thereby contributing solely to PFR. When integrated with battery energy storage systems (BESS), they can leverage an additional RoCoF-based control loop, allowing for rapid energy injection that emulates the inertial response of synchronous machines while maintaining sustained PFR. This dual-loop control approach enhances grid stability by mitigating RoCoF and ensuring frequency nadir remains within acceptable limits. Single loop and dual loops controller schemes for GFMs are shown in Figure 2.

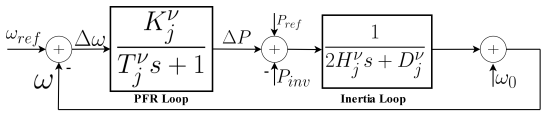

Fig. 2: GFM dual loop control

D. Dynamic Frequency Constraints (DFCs) Formulation

To integrate the diverse frequency support capabilities of different generation technologies, we derive the following DFC constraints. Assuming a disturbance ΔP_{cont} occurs at $t = t_0$, the post-contingency power-frequency dynamics can be modeled by the swing equation:

$$\begin{aligned}\sum_i \Delta P_i^{SG,PFR} + \sum_j \Delta P_j^{\nu,PFR} - \Delta P_{cont} \\ = \frac{2H_{\text{sys}}}{f_0}\frac{d\Delta f_t}{dt} + K^D \Delta f_t\end{aligned} \tag{7}$$

ΔP_i^{PFR} is the PFR response from the i^{th} investment technology while $\Delta P_j^{\nu,PFR}$ is the PFR like response from the j^{th} renewable resource. where H^{sys} represents the total system inertia, given by:

$$H_{\text{sys}} = \sum_i H_i^{SG} + \sum_j H_j^{\nu} \tag{8}$$

where $\sum_i H_i^S$ is the contribution from SGs into inertial response while $\sum_j H_j^\nu$ is that from VREs. The first two terms in (7) denote the PFR contributions from SGs and VREs respectively. The right hand side of the equation addresses the IR response from both SGs and VREs, while the last term accounts for load damping characteristics (LDC).

The PFR dynamics are given by:

$$\begin{aligned}T_i^{SG}\frac{d\Delta P_i^{SG,PFR}}{dt} + \Delta P_i^{SG,PFR} = K_i^{SG}\Delta f_t, \\ T_j^{\nu}\frac{d\Delta P_j^{\nu,PFR}}{dt} + \Delta P_j^{\nu,PFR} = K_j^{\nu}\Delta f_t\end{aligned} \tag{9}$$

where T_j^ν is significantly smaller than T_i^{SG} , and can be approximated as zero [5]. Additionally, the inertia and droop characteristics of VRE are assumed to be responsive as long as sufficient headroom is available.

1) RoCoF Constraint Considering Inertia Diversities: The maximum Rate of Change of Frequency (RoCoF) occurs immediately after the disturbance, at $t = t_0^+$, when no PFR has yet been activated . Setting $\Delta f = 0$ in the swing equation, we obtain:

$$\Delta P_{cont} = \frac{2H_{\text{sys}}}{f_0}\frac{d\Delta f_t}{dt}\Big|_{t=t_0^+} \tag{10}$$

By substituting (8) into (10), the maximum RoCoF can be expressed as:

$$\overline{RoCoF} = \frac{d\Delta f_t}{dt}\Big|_{t=t_0^+} = \frac{\Delta P_{cont} f_0}{2\left(\sum_i H_i^{SG} + \sum_j H_{j,k}^{\nu}\right)} \tag{11}$$

Since increased system inertia reduces the maximum RoCoF, investment decisions must allocate sufficient inertia to limit RoCoF deviations:

$$\sum_i H_i^{SG} + \sum_j H_{j,k}^{\nu} \geq \frac{\Delta P_{cont} f_0}{2\overline{RoCoF}} \tag{12}$$

2) Frequency Nadir Constraint Considering PFR Ramping Capabilities: In a critical security scenario , the system frequency reaches its minimum threshold (nadir) at time $t = t_n$, where:

$$\Delta f_{t_n} = \overline{\Delta f}, \quad \frac{d\Delta f_t}{dt}\Big|_{t=t_n} = 0 \tag{13}$$

Substituting these conditions into the swing equation:

$$\Delta P_{cont} = \sum_i \Delta P_{i_n}^{G,PFR} + \sum_j K_{j,k}^{\nu} \Delta f + K^D \Delta f \tag{14}$$

Rearranging, the frequency nadir constraint can be derived as:

$$\Delta P_{cont} \leq \sum_i \Delta P_{i_n}^{G,PFR} + \sum_j K_{j,k}^{\nu} \Delta f + K^D \Delta f \tag{15}$$

This ensures sufficient PFR ramping capability to stabilize the frequency before it falls below the nadir threshold. Here, $\Delta P_{i_n}^{G,PFR}$ represents the PFR capacity of generator i at nadir, but its precise value remains uncertain because of the different ramping capabilities.

3) QSS Frequency Constraint Considering Quasi-Steady-State (QSS) PFR Power Diversities: At quasi-steady-state (QSS) , as $t \to \infty$, RoCoF vanishes and inertial response ceases:

$$\frac{df_t}{dt}\Big|_{t=\infty} = 0, \quad \Delta f_\infty = \Delta f^{ss} \tag{16}$$

Applying these conditions to the swing equation:

$$\Delta P_{cont} = \sum_i K_i^{SG} \Delta f^{ss} + \sum_j K_{j,k}^{\nu} \Delta f^{ss} + K^D \Delta f^{ss} \tag{17}$$

From this, the steady-state frequency deviation is:

$$\Delta f^{ss} = \frac{\Delta P_{cont}}{\sum_i K_i^{SG} + \sum_j K_{j,k}^{\nu} + K^D} \tag{18}$$

To ensure frequency security, investment decisionshould account for QSS PFR variations :

$$\Delta P_{cont} \leq \Delta \overline{f^{ss}} \left(\sum_i K_i^{SG} + \sum_j K_{j,k}^{\nu} + K^D \right) \tag{19}$$

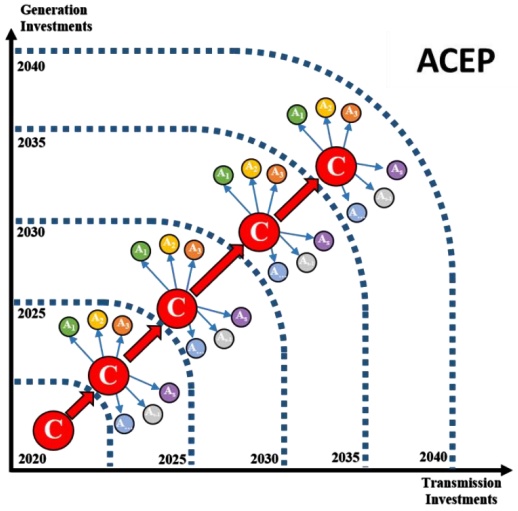

Fig. 3: Illustration of the cost function of ACEP, which includes both a core cost and adaptation costs

III. DFC-ACEP Formulation

The DFC-ACEP optimization problem is formulated to ensure system frequency stability while adhering to predefined standards and accounting for the diversity of generation technologies and their respective capabilities, as governed by the previously established constraints. Simultaneously, the DFC-ACEP framework aims to minimize total costs.

Figure 3 illustrates the expansion planning process over the considered time horizon. The core cost (C), highlighted by red circles, signifies the primary investment costs associated with each planning year. Each core cost is linked to additional smaller circles labeled A_i, representing operational costs and adaptation costs, which vary depending on system conditions and uncertainties. These additional costs are assigned probabilities, reflecting their likelihood of occurrence. The structure of the diagram highlights the iterative nature of DFC-ACEP, where decisions at each stage influence future investments in both generation and transmission expansion, ensuring an optimal and resilient long-term planning strategy. The objective function is expressed as:

$$\min\left\{x + \beta \sum P_k \times \Delta \underline{x} + \sum P_k \times \Delta x\right\} \tag{20}$$

where: x represents a given year expansion plan cost, while k denotes a possible future scenario among the n total considered futures. β is a robustness constant that governs the trade-off between core investment costs and adaptation costs. subject to the following constraints:

$$\sum_i H_i S_{B,i} \geq \frac{30 \Delta P_{\text{cont}}^{max}}{\text{ROCOF}_{\text{max}}} \tag{21}$$

In (21), it is ensured that a sufficient system inertia exists to limit RoCoF violations and maintain frequency stability.

For the system to maintains the required primary frequency response capability, a PFR constraint is imposed as in 22.

$$\sum_{g,t} pfr_{g,t} \geq \text{PFR}_{\text{req}}, \quad \forall g,t \tag{22}$$

$$P_{g,t} + pfr_{g,t} \leq P_{g,\max}, \quad \forall g,t \tag{23}$$

The total power output of a generator cannot not exceed its rated capacity as given in (23). Whilst (24) limits the generator's frequency response to its ramping capability.

$$pfr_{g,t} \leq \mu PFRR_{g,\max}, \quad \forall g,t \tag{24}$$

$$\begin{aligned} P_{g,t} + pfr_{g,t} + P_{\text{Reg},g,t} + P_{\text{Cont},g,t} \\ + P_{\text{RampUp},g,t} + P_{\text{STR},g,t} \leq P_{g,\max}, \quad \forall g,t \end{aligned} \tag{25}$$

Eq. (25) ensures total reserve and generation commitments do not exceed generation limits.

$$P_{g,t} - P_{\text{RampDn},g,t} \geq P_{g,\min}, \quad \forall g,t \tag{26}$$

Maintains minimum operational limits for each generator.

$$\sum_{g,t} P_{\text{Cont},g,t} \geq \text{LSSC}, \quad \forall g,t \tag{27}$$

Requires contingency reserves to be at least the largest single system contingency.

$$P_{\text{Cont},g,t} \leq \mu_{\text{Cont}} R_{g,\max}, \quad \forall g,t \tag{28}$$

Limits contingency reserve contributions based on generator ramping capabilities.

$$\sum_{g,t} P_{\text{Reg},g,t} \geq \text{Total Required Regulating Reserve}, \quad \forall g,t \tag{29}$$

Ensures sufficient regulating reserves to balance short-term system deviations.

$$P_{\text{Reg},g,t} \leq \mu_{\text{Reg}} R_{g,\max}, \quad \forall g,t \tag{30}$$

Ensures regulation reserves do not exceed ramping limits.

$$\sum_{g,t} P_{\text{RampUp},g,t} \geq \text{Total Required Ramp Up Reserve}, \quad \forall g,t \tag{31}$$

Maintains sufficient ramp-up reserves to accommodate demand increases.

$$P_{\text{RampUp},g,t} \leq \mu_{\text{RampUp}} R_{g,\max}, \quad \forall g,t \tag{32}$$

Limits ramp-up reserves based on generation ramp rates.

$$\sum_{g,t} P_{\text{RampDn},g,t} \geq \text{Total Required Ramp Down Reserve}, \quad \forall g,t \tag{33}$$

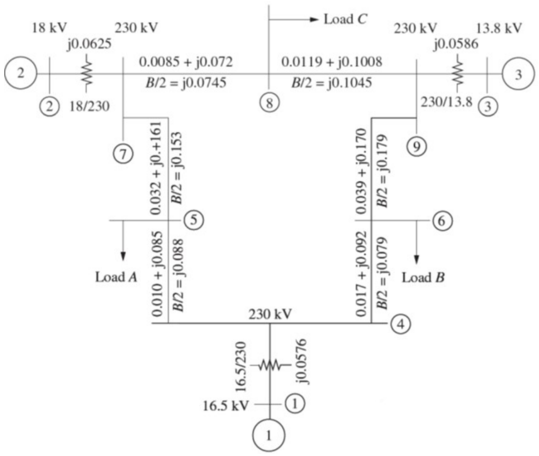

Fig. 4: The nine-bus test system

Ensures ramp-down reserves are available to handle demand reductions.

$$P_{\text{RampDn},g,t} \leq \mu_{\text{RampDn}} R_{g,\max}, \quad \forall g,t \tag{34}$$

Limits ramp-down reserves based on ramping capabilities.

$$\sum_{g,t} P_{\text{STR},g,t} \geq \text{Total Required Short-Term Reserve}, \quad \forall g,t \tag{35}$$

Ensures sufficient short-term reserves are available for fast response needs.

$$P_{\text{STR},g,t} \leq \mu_{\text{STR}} R_{g,\max}, \quad \forall g,t \tag{36}$$

Limits short-term reserve contributions to feasible generator response levels.

These constraints ensure that system stability, frequency response, and reserve adequacy are maintained while optimizing economic efficiency.

IV. Case Studies and Simulation Results

The simulation framework is based on the IEEE 9-bus test system, comprising three synchronous generation sites and three load buses, as illustrated in Fig. 4. The objective of this study is to investigate the sensitivity of key frequency stability metrics—namely,RoCoF, frequency nadir, and time to nadir—with respect to changes in system inertia and control strategies. The analysis begins with high- and low-inertia configurations under equivalent generation-loss disturbances to quantify the impact of reduced kinetic energy. Subsequently, a staged replacement of synchronous machines with IBRs is performed. Two IBR control configurations are examined: (1) constant-power operation without frequency support, and (2) IBRs equipped with synthetic inertia and virtual droop control.

The contribution of these controlled IBRs is interpreted as a form of fast frequency response (FFR), analogous to PFR traditionally provided by synchronous machines. The effectiveness of the emulated inertia and droop mechanisms

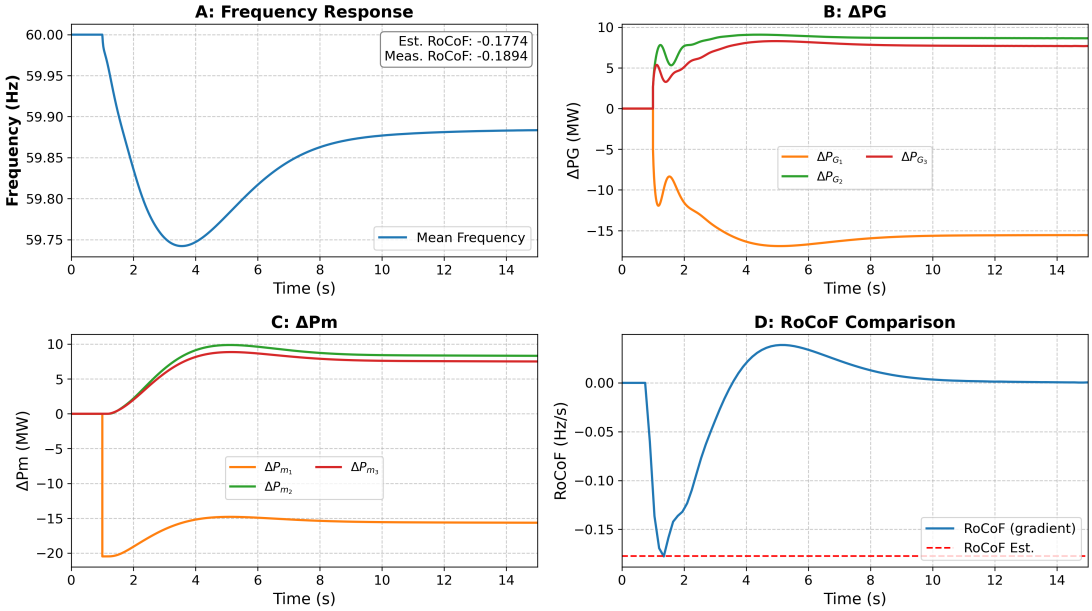

Fig. 5: Frequency response analysis for the base case; scnearios#1. Subplots include: (A) system-wide frequency response (f_{COI}); (B) change in generator active power; (C) primary frequency response (PFR); and (D) comparison between measured and estimated RoCoF.

TABLE II: Modular Unit Configuration and Inertia Constants

Bus	# Units (Capacity Each)	Scenario#1 H (s)	Scenario#2 H (s)
1	13 (20 MW) = 260 MW	9.55	0.9286
2	12 (20 MW) + 2 (35 MW) = 310 MW	3.33	0.9286
3	14 (20 MW) = 280 MW	2.35	0.9286

is quantified by comparing frequency response metrics against those of the original synchronous case, highlighting the potential of IBRs to compensate for lost inertial and governor-based support.

A. System Configuration and Modularization Framework

To facilitate detailed dynamic assessment of system inertia and generator response characteristics, the IEEE 9-bus test system was modified by disaggregating each of the three synchronous generators into multiple modular generation units with their ratings shown in Table II. This modular representation retains the aggregate power output and steady-state characteristics of the original system but enables fine-grained control over contingency events such as selective generator tripping and progressive replacement with IBRs. Each original generator bus was partitioned into two newly created low-voltage buses: the first consistently hosts modular synchronous generator units, while the second accommodates either additional synchronous units or IBRs, depending on whether a penetration scenario involving IBRs is being studied. Thereby enhancing the spatial resolution for studying inertia placement and synthetic inertia deployment.

B. Frequency Response under High and Low Inertia Conditions

Two baseline scenarios were simulated to evaluate the impact of inertia on system frequency dynamics. In the first scenario—denoted as Scenario#1 in Table II—the system preserves the original inertia constants assigned to the synchronous generators in the conventional configuration. A generation trip event corresponding to 20 MW was simulated, and the RoCoF was estimated analytically based on the known system-wide inertia and disturbance size. This estimate was validated against the measured RoCoF from time-domain simulation using a 0.5-second finite difference window. Results, as shown in Fig. 5 indicate close agreement between analytical and measured RoCoF values, confirming the validity of the estimation method under nominal inertia conditions. The center-of-inertia (COI) frequency exhibited a smooth decline, with active power output rising immediately post-contingency and mechanical power following more gradually due to governor response.

In the second scenario, the inertia constants of all modular synchronous units were uniformly reduced, resulting in a total system inertia decrease of approximately 3400 MW·s as detailed in Table II. Under this low-inertia condition, the frequency response showed a significantly steeper initial decline and increased oscillatory behavior. The RoCoF was substantially higher compared to scenario#1, and the system frequency nadir was both lower and occurred earlier as depicted in Fig. 6. These results underscore the importance of system inertia in shaping both the magnitude and temporal characteristics of frequency deviations following disturbances. The two scenarios are evaluated under multiple tripping conditions, revealing a pronounced impact of system inertia on key

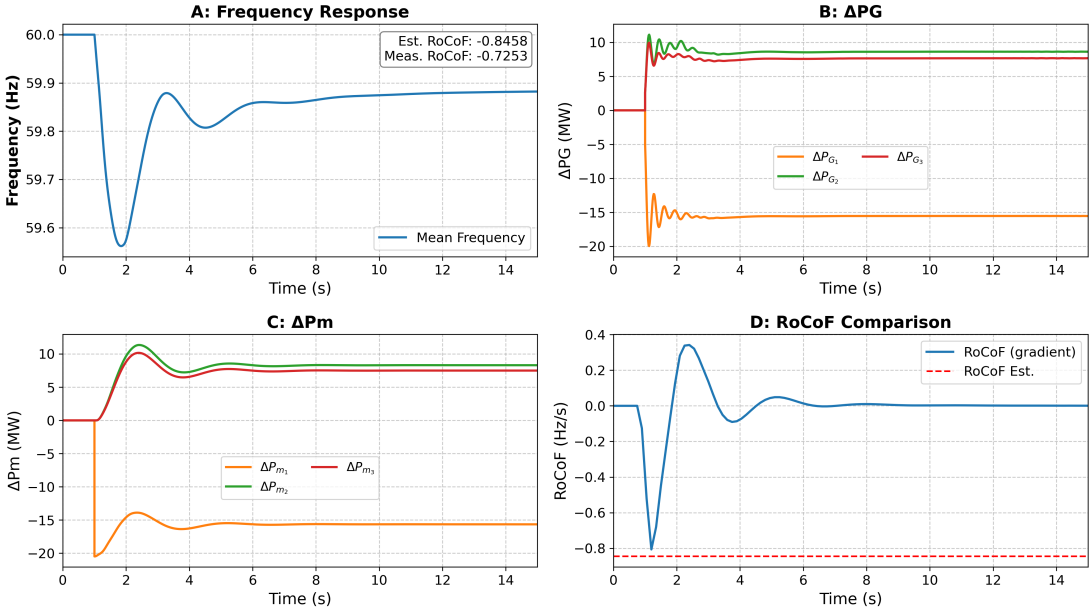

Fig. 6: Frequency response analysis for the base case; scnearios#2. Subplots include: (A) system-wide frequency response (f_{COI}); (B) change in generator active power; (C) primary frequency response (PFR); and (D) comparison between measured and estimated RoCoF.

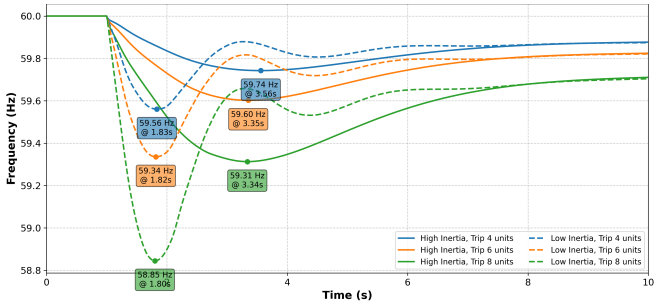

Fig. 7: Impact of system inertia on frequency nadir, time to nadir, and RoCoF under varying generator tripping sizes.

frequency response metrics, including frequency nadir, time to nadir, and RoCoF, as illustrated in Fig. 7. The results in Fig. 8 highlight the sensitivity of frequency response metrics to system inertia. Under reduced inertia conditions, the observed and predicted RoCoF increase substantially, frequency nadirs become deeper, and the system reaches nadir more quickly. These results validate the analytical RoCoF estimation and illustrate how low inertia impairs the system's ability to arrest frequency deviations during disturbance events.

C. Progressive Replacement with Inverter-Based Resources and Synthetic Inertia Control

Building upon the modularized system framework, a progressive replacement strategy was implemented to evaluate the impact of increasing IBR penetration. Selected modular synchronous units were replaced with IBRs of equivalent rating. In the first case, the IBRs were modeled as constant power devices without any frequency support, resulting in degraded frequency response metrics across all evaluated tripping scenarios. In the second scenario, auxiliary control signals derived from the point-of-interconnection (POI) frequency measurements are integrated into the power control loops of IBRs, enabling synthetic inertia and droop control emulation according to assigned parameters. This closed-loop control allows IBRs to contribute actively to frequency stabilization. The corresponding dynamic response of both synchronous and inverter-based units under a 30% IBR penetration level is illustrated in Fig. 9. The figure demonstrates the coordinated active power injection from IBRs in response to system frequency deviations, where the auxiliary power signal (P_{aux}) evolves according to the assigned synthetic inertia parameters. This control action effectively contributes to RoCoF mitigation following the disturbance.

Figure 10 presents a comparative analysis of frequency response metrics—observed RoCoF, frequency nadir, and time to nadir—under varying tripping scenarios for three configurations: (i) only synchronous generation, (ii) 30% IBR penetration without frequency control, and (iii) 30% IBR penetration with GFL control. In the uncontrolled IBR case, the reduced system inertia leads to significantly higher RoCoF magnitudes and lower nadir values, highlighting the vulnerability of low-inertia systems to sudden generation loss. However, when IBRs are equipped with synthetic inertia and droop-based active power support, the RoCoF is effectively reduced, and the frequency nadir is improved across all tripping sizes.

Importantly, the controlled IBR case exhibits frequency dynamics closely aligned with the purely synchronous generation case (with respect to RoCoF), indicating that appropriately designed FFR strategies can enable IBRs to mimic the inertial behavior of synchronous machines. This result emphasizes the critical role of IBR control design in enhancing grid resilience

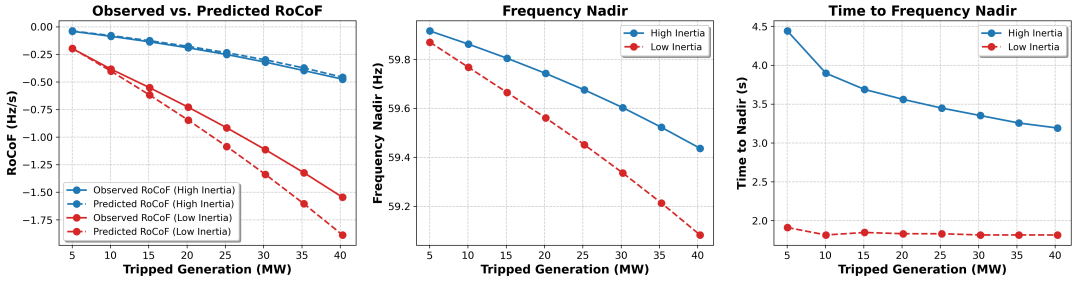

Fig. 8: Comparison of RoCoF, frequency nadir, and time to nadir under high and low inertia scenarios with synchronous generation only.

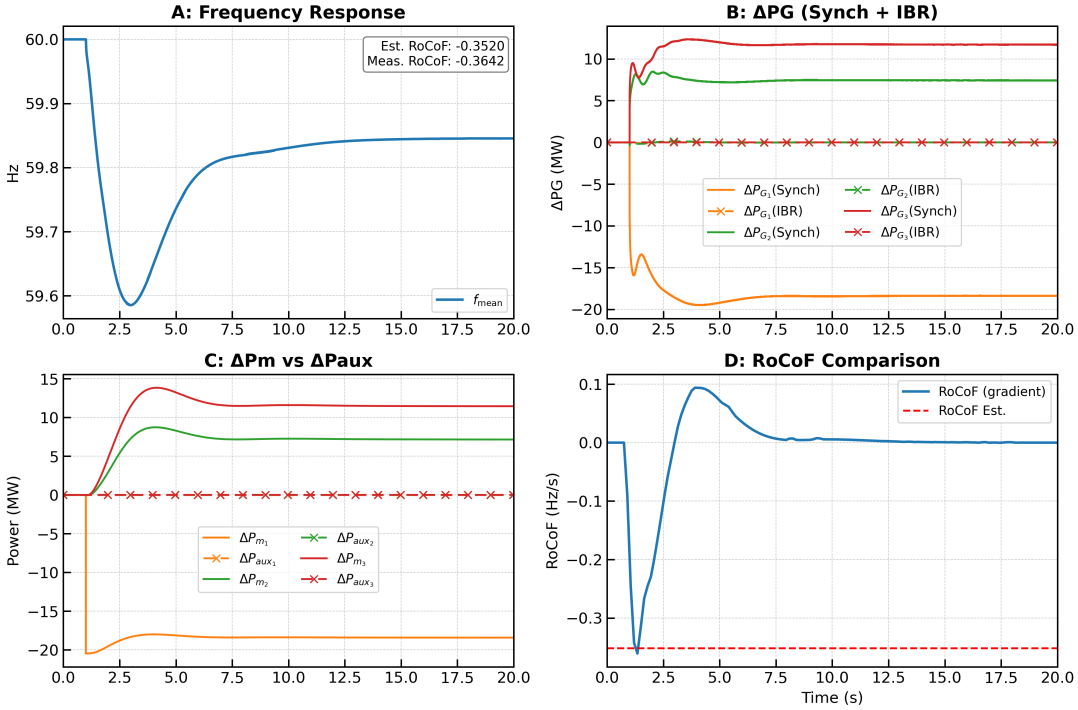

Fig. 9: System frequency response and active power contribution from synchronous machines and IBRs under 30% penetration level with synthetic inertia and droop control enabled.

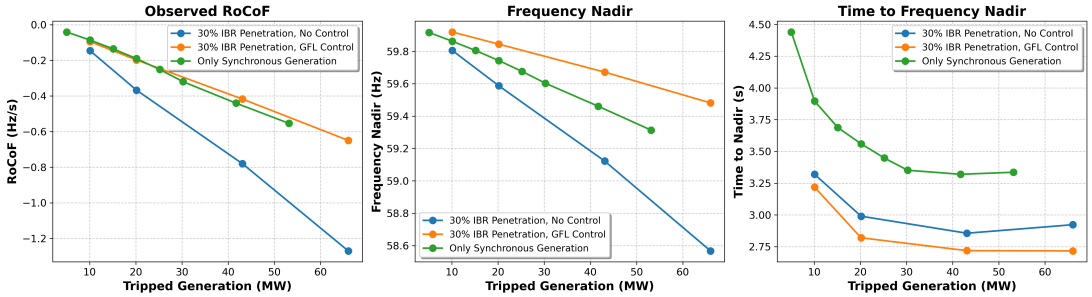

Fig. 10: Comparison of frequency response metrics under multiple tripping scenarios for three cases: only synchronous generation, 30% IBR penetration without control, and 30% IBR penetration with GFL control. The implementation of synthetic inertia and droop control enables IBRs to emulate the inertial behavior of synchronous machines, effectively reducing RoCoF and improving frequency nadir recovery.

under high renewable penetration scenarios.

V. Conclusion

As power systems integrate higher shares of renewable energy, maintaining frequency stability becomes increasingly complex. This paper emphasizes the necessity of embedding security constraints within the proposed long-term expansion planning framework, DFC-ACEP, to ensure a reliable and resilient dynamic frequency response. The proposed approach enables cost-effective investments in a diverse generation mix while guaranteeing compliance with frequency stability standards under contingency conditions. By leveraging a coordinated combination of synchronous inertia, PFR, synthetic inertia, and fast FFR from IBRs, the framework enhances the system's frequency resilience in the face of disturbances.

Appendix A
System Frequency Dynamics Model

We start from the fundamental frequency dynamics, represented by the swing equation:

$$G_{sw}(s) = \frac{1}{2H^{SG}s + K^D} \tag{37}$$

where $\Delta f(s)$ is the Laplace transform of frequency deviation, $\Delta P_{cont}(s)$ is the electrical power disturbance, $M^{SG} = 2H^{SG}$ is the aggregated system synchronous inertia constant, and K^D is the aggregated load damping coefficient.

Frequency support from synchronous generators (SGs), grid-following (GFL), and grid-forming (GFM) inverter-based resources (IBRs) is modeled as feedback control. The feedback transfer functions are defined as:

a) Synchronous Generators (SGs):

$$G_{\text{SG}}(s) = \sum_{i=1}^{n_g} \frac{K_{g,i}}{T_{g,i}s + 1} \tag{38}$$

b) Grid-Following (GFL) IBRs:

$$G_{\text{GFL}}(s) = \sum_{j=1}^{n_{GFL}} \frac{2H_{v,j}s + K_{v,j}}{T_{v,j}s + 1} \tag{39}$$

c) Grid-Forming (GFM) IBRs:

$$G_{\text{GFM}}(s) = \sum_{q=1}^{n_{GFM}} (2H_{v,q}s + K_{v,q}) \tag{40}$$

Combined total feedback:

$$G_{\text{PFR,total}}(s) = G_{\text{SG}}(s) + G_{\text{GFL}}(s) + G_{\text{GFM}}(s) \tag{41}$$

Closed-loop transfer function:

$$\frac{\Delta f(s)}{\Delta P_e(s)} = \frac{G_{\text{sw}}(s)}{1 + G_{\text{sw}}(s)G_{\text{PFR,total}}(s)} \tag{42}$$

Substituting (37):

$$\frac{\Delta f(s)}{\Delta P_e(s)} = \frac{1}{Ms + D + \sum G_{\text{SG}} + \sum G_{\text{GFL}} + \sum G_{\text{GFM}}} \tag{43}$$

With common denominators applied, this expands to:

TABLE III: Equations Defining Key Parameters

ω_n	$\sqrt{\frac{D+R}{MT}}$
ζ	$\frac{M+T(D+F)}{2\sqrt{MT(D+R)}}$
M	$\frac{\sum M_i^{SG} S_{b,i}^{SG} + \sum 2H_j^{\nu gfl} S_{b,j}^{\nu gfl}}{\sum S_{b,i}^{SG} + \sum S_{b,i}^{\nu gfl}}$
D	$\frac{\sum D_{sg,i} S_{sg,i} + \sum D_{ibr,i} S_{ibr,i}}{\sum S_{sg,i} + \sum S_{ibr,i}}$
F	$\frac{\sum \frac{K_{sg,i} F_{sg,i} S_{sg,i}}{R_{sg,i}}}{\sum S_{sg,i}}$
R	$\frac{\sum \frac{K_{sg,i} S_{sg,i}}{R_{sg,i}}}{\sum S_{sg,i}}$

$$\frac{\Delta f(s)}{\Delta P_e(s)} = \frac{\prod_i (T_{g,i}s + 1) \prod_j (T_{v,j}s + 1)}{(Ms + D) \prod_i (T_{g,i}s + 1) \prod_j (T_{v,j}s + 1)} + F_{\text{SG}}(s) + F_{\text{GFL}}(s) + F_{\text{GFM}}(s) \tag{44}$$

Where:

$$F_{\text{SG}}(s) = \sum_i K_{g,i} \prod_{m \neq i} (T_{g,m}s + 1) \prod_j (T_{v,j}s + 1) \tag{45}$$

$$F_{\text{GFL}}(s) = \sum_j (2H_{v,j}s + K_{v,j})(Ms + D) \times \prod_{k \neq j} (T_{v,k}s + 1) \prod_i (T_{g,i}s + 1) \tag{46}$$

$$F_{\text{GFM}}(s) = (2H_{v,\text{GFM}}^{eq}s + K_{v,\text{GFM}}^{eq})(Ms + D) \times \prod_i (T_{g,i}s + 1) \prod_j (T_{v,j}s + 1) \tag{47}$$

With equivalent:

$$2H_{v,GFM}^{eq}s + K_{v,GFM}^{eq} = \sum_q (2H_{v,q}s + K_{v,q}) \tag{48}$$

Under assumption of identical SG time constants and fast IBR response:

$$G(s) = \frac{1}{MT} \frac{1 + sT}{s^2 + 2\zeta\omega_n s + \omega_n^2} \tag{49}$$

A. Analytical Frequency Response

$$\Delta f(s) = \frac{\Delta P_e}{MT} \frac{1 + sT}{s(s^2 + 2\zeta\omega_n s + \omega_n^2)} \tag{50}$$

$$\Delta f(t) = \frac{\Delta P_e}{MT\omega_n^2} \left[1 - e^{-\zeta\omega_n t} \eta \sin(\omega_d t + \phi)\right] \tag{51}$$

$$\omega_d = \omega_n \sqrt{1-\zeta^2} \tag{52}$$

(53)

$$\eta = \frac{\sqrt{1-2T\omega_n\zeta+T^2\omega_n^2}}{\sqrt{1-\zeta^2}} \tag{54}$$

(55)

$$\tan\phi = \frac{\omega_d}{-T\omega_n^2+\zeta\omega_n} \tag{56}$$

Nadir:

$$\Delta f_{\text{nadir}} = \frac{\Delta P_e}{MT\omega_n^2}\left[1-\sqrt{1-\zeta^2}\eta e^{-\zeta\omega_n t_m}\right] \tag{57}$$

RoCoF at $t = 0^+$:

$$\dot{f}_{max} = \left.\frac{d\Delta f}{dt}\right|_{0^+} = -\frac{\Delta P_e}{M} \tag{58}$$

B. Analytical Power Response of IBRs

$$\Delta P_{ibr}(s) = \frac{\Delta P_e}{MT}\frac{(M_{ibr}s+D_{ibr})(1+sT)}{s(s^2+2\zeta\omega_n s+\omega_n^2)} \tag{59}$$

$$\Delta P_{ibr}(s) = \frac{\Delta P_e D_{ibr}}{MT\omega_n^2}\left(-\frac{1}{s}+\frac{\alpha s+\beta}{s^2+2\zeta\omega_n s+\omega_n^2}\right) \tag{60}$$

$$\alpha = 1-\frac{M_{ibr}T\omega_n^2}{D_{ibr}}, \quad \beta = \frac{-T\omega_n^2+2\zeta\omega_n-M_{ibr}\omega_n^2}{D_{ibr}} \tag{61}$$

$$\Delta P(t) = \frac{\Delta P_e D_{ibr}}{MT\omega_n^2}\left[-1+\alpha\eta' e^{-\zeta\omega_n t}\sin(\omega_d t+\phi')\right] \tag{62}$$

$$\tan\phi' = \frac{\omega_d}{\beta/\alpha-\zeta\omega_n}, \quad \eta' = \sqrt{1+\left(\frac{\beta/\alpha-\zeta\omega_n}{\omega_d}\right)^2} \tag{63}$$

$$\left.\frac{d\Delta P_{\text{ibr}}(t)}{dt}\right|_{t=t_m} = 0 \tag{64}$$

$$t_m = \frac{1}{\omega_d}\tan^{-1}\left(\frac{(\beta-2\zeta\alpha\omega_n)\omega_d}{\zeta\beta\omega_n-\zeta^2\omega_n^2+\alpha\omega_d^2}\right) \tag{65}$$

$$\Delta P_{\text{peak}} = \frac{\Delta P_e D_{\text{ibr}}}{MT\omega_n^2}\left[-1+\alpha\eta\left(1-\zeta^2 e^{-\zeta\omega_n t_m}\right)\right] \tag{66}$$

IBR Inertia and PFR Headroom

$$\Delta P_{\text{peak}} = \frac{\Delta P_e D_{\text{ibr}}}{MT\omega_n^2}\left[-1+\alpha\eta\left(1-\zeta^2 e^{-\zeta\omega_n t_m}\right)\right] \tag{67}$$

REFERENCES

[1] B. She, F. Li, H. Cui, J. Wang, Q. Zhang, and R. Bo, "Virtual inertia scheduling (vis) for real-time economic dispatch of ibr-penetrated power systems," *IEEE Transactions on Sustainable Energy*, vol. 15, no. 2, pp. 938–951, 2023.

[2] J. L. Jorgenson and P. L. Denholm, "Modeling primary frequency response for grid studies," National Renewable Energy Laboratory (NREL), Golden, CO (United States), Tech. Rep., 2019.

[3] E. Ela, V. Gevorgian, A. Tuohy, B. Kirby, M. Milligan, and M. O'Malley, "Market designs for the primary frequency response ancillary service—part i: Motivation and design," *IEEE Transactions on Power Systems*, vol. 29, no. 1, pp. 421–431, 2013.

[4] Y. Liu, R. Huang, W. Du, A. Singhal, and Z. Huang, "Highly-scalable transmission and distribution dynamic co-simulation with 10,000+ grid-following and grid-forming inverters," *IEEE Transactions on Power Delivery*, vol. 39, no. 1, pp. 578–590, 2023.

[5] Z. Zhang, M. Zhou, Z. Wu, S. Liu, Z. Guo, and G. Li, "A frequency security constrained scheduling approach considering wind farm providing frequency support and reserve," *IEEE Transactions on Sustainable Energy*, vol. 13, no. 2, pp. 1086–1100, 2022.